Regulation of spine morphology and spine density by NMDA receptor signaling *in vivo*

Sila K. Ultanir*, Ji-Eun Kim*, Benjamin J. Hall*, Thomas Deerinck†, Mark Ellisman†, and Anirvan Ghosh*‡

*Neurobiology Section, Division of Biological Sciences, and †National Center for Microscopy and Imaging Research, Center for Research in Biological Systems, University of California at San Diego, La Jolla, CA 92093

Edited by Charles F. Stevens, Salk Institute for Biological Studies, La Jolla, CA, and approved October 11, 2007 (received for review May 2, 2007)

Dendritic spines are the major sites of excitatory synaptic transmission in the CNS, and their size and density influence the functioning of neuronal circuits. Here we report that NMDA receptor signaling plays a critical role in regulating spine size and density in the developing cortex. Genetic deletion of the NR1 subunit of the NMDA receptor in the cortex leads to a decrease in spine density and an increase in spine head size in cortical layer 2/3 pyramidal neurons. This process is accompanied by an increase in the presynaptic axon bouton volume and the postsynaptic density area, as well as an increase in the miniature excitatory postsynaptic current amplitude and frequency. These observations indicate that NMDA receptors regulate synapse structure and function in the developing cortex.

cortex | development | synapse

Dendritic spines are bulbous membrane protrusions that form the postsynaptic specializations of the vast majority of excitatory synapses in the CNS (1–3). During the first postnatal week, highly motile and short-lived dendritic filopodia are abundant on cortical pyramidal neurons (4). These actin-rich protrusions make immature synapses along their length or tip (5). The dendritic spines that are present during the first two postnatal weeks display an immature morphology (5), and the spine head is highly motile, with protrusions extending and retracting from the head (6). After the second postnatal week, the spine density increases, and spines attain a mature morphology with bulbous heads similar to that seen in the adult (7). Dendritic spines are sites of excitatory synaptic transmission, and their structure and density are important measures of synaptic function.

An important feature of dendritic spines is that their volume and density can be dynamically regulated. Stimuli that induce long-term potentiation (LTP) and long-term depression in hippocampal slices lead to rapid changes in spine volume by activation of NMDA receptors (8–10). Several lines of evidence suggest that NMDA receptor signaling might influence spine volume by recruitment of AMPA receptors (AMPARs). Immature synapses in the CNS have a low AMPAR:NMDA receptor (NMDAR) ratio and gradually acquire AMPARs during development (11, 12). The increase in the AMPAR:NMDAR ratio at synapses during development is thought to be mediated by NMDAR-induced recruitment of AMPARs (13–16). This increase in surface AMPARs could influence spine volume because it has been reported that overexpression of the GluR2 AMPAR subunit in hippocampal cultures leads to an increase in spine size (17). NMDAR signaling also has been implicated in regulating spine density. In hippocampal slices, LTP-inducing stimuli or glutamate application leads to the rapid induction of new spines/filopodia, which is blocked by NMDAR antagonists (18, 19).

These observations suggest a model in which NMDARs recruit AMPARs to developing synapses, which drives spine growth and maturation. This model predicts that loss of NMDARs should lead to smaller AMPA currents and smaller spines. Here we present evidence that this model does not strictly apply to developing synapses *in vivo*. We base our conclusions on the analysis of mice in which NMDARs were genetically deleted from the cortex. These mice are viable, but display major defects in their synaptic organization. We focused our analysis on layer 2/3 pyramidal neurons because the synaptic organization of these neurons is well characterized and has been studied extensively in the context of NMDAR-dependent developmental plasticity. We report that layer 2/3 pyramidal neurons in cortical NR1-null mice have fewer, but larger, spines. They receive larger AMPAR miniature excitatory postsynaptic currents (mEPSCs) with higher frequency. In addition, synapses in NR1-null mice have larger postsynaptic densities (PSD) and larger presynaptic boutons. On the basis of these findings, we propose that NMDAR signaling increases spine density, but restricts AMPAR recruitment and spine growth in developing neurons.

Results

To generate cortical NR1 KO mice, we crossed NR1-floxed mice (20) to Nex-Cre mice, which express Cre recombinase under Nex promoter in postmitotic pyramidal neurons in the cortex and hippocampus (21, 22). Because NR1 is the obligatory subunit of the NMDAR, cortical pyramidal neurons in this KO lack NMDAR postnatally (21, 22). Western blot of protein lysates from postnatal day 10 (P10) and P19 cortices shows a marked reduction of NR1 protein in these mice [supporting information (SI) Fig. 6]. The residual NR1 expression most likely reflects NR1 expression in interneurons and glia, which are not affected by Nex-Cre-mediated recombination. Consistent with previous observations (23), we also observed a reduction in NR2A and NR2B protein levels, indicating that expression and stability of these subunits depend on functional NR1 subunits (SI Fig. 6).

Cortical NR1-null mice are viable, but smaller than control littermates (Fig. 1*A*). Their brains do not display gross histological abnormalities (Fig. 1 *A* and *B*), but most of these mice do not survive past P24. To determine whether the organization of the cortex was affected in cortical NR1-null mice, we examined the development of whisker-associated barrels in these mice. In control animals, barrels representing individual whiskers are clearly distinguishable by cytochrome oxidase or Hoechst 33342 staining of tangential sections through layer 4 of the somatosensory cortex (Fig. 1*C*). In mice lacking cortical NR1, there was a striking absence of barrels, indicating that cortical NMDAR function was required for normal patterning of thalamocortical connections (Fig. 1*C*).

To determine whether loss of NMDARs affected the development of synaptic currents, we examined evoked responses in

Author contributions: S.K.U., M.E., and A.G. designed research; S.K.U., J.-E.K., B.J.H., and T.D. performed research; S.K.U., J.-E.K., B.J.H., M.E., and A.G. analyzed data; and S.K.U., T.D., M.E., and A.G. wrote the paper.

The authors declare no conflict of interest.

This article is a PNAS Direct Submission.

‡To whom correspondence should be addressed. E-mail: aghosh@ucsd.edu.

This article contains supporting information online at www.pnas.org/cgi/content/full/0704031104/DC1.

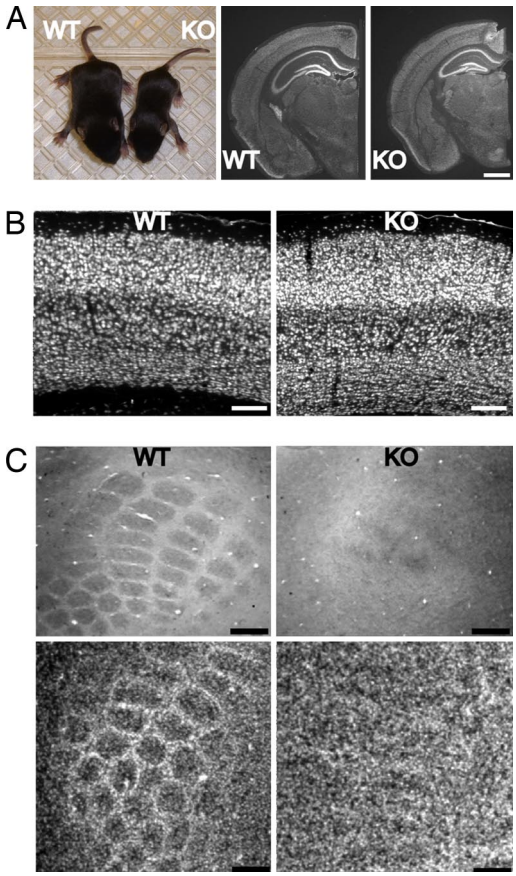

Fig. 1. Characterization of cortical NR1-null mice. (*A*) (*Left*) P9 littermate WT and cortical NR1 KO (Nex-Cre × floxed NR1) mice. The KO mice weigh 30% less than their WT littermates, and their brain size is slightly smaller. (*Right*) Coronal forebrain sections from WT and cortical NR1 KO mice at P16 stained for a neuronal nuclear marker (NeuN). (Scale bar: 1 mm.) (*B*) Cortical sections from WT and cortical NR1-null mice, stained with an antibody to NeuN. Cortical layers are visible in both KO and WT. (Scale bars: 200 μm.) (*C*) (*Upper*) Cytochrome oxidase staining of tangential sections through layer 4 of WT and cortical NR1-null mice at P19. Note the absence of whisker-associated barrels in the KO mice. (Scale bars: 150 μm.) (*Lower*) Visualization of barrel field in tangential sections from WT and NR1-null mice by Hoechst staining. Neuronal cell bodies do not segregate into barrels in layer 4 in the KO. (Scale bars: 100 μm.)

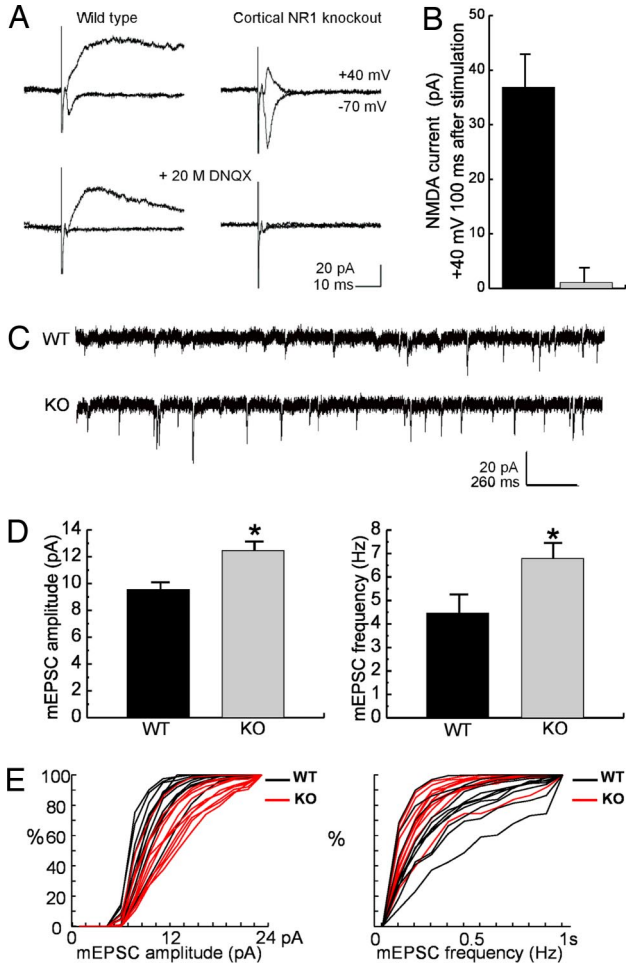

Fig. 2. Effect of loss of NMDAR function on development of AMPAR-mediated synaptic currents. (*A*) Traces are whole-cell, voltage–clamp recordings in acute slices prepared from P9 cortex. Responses were measured in layer 2/3 pyramidal neurons after stimulation of layer 4. (*Left*) WT neurons display a rapid DNQX-sensitive current at −70 mV, typical of AMPAR-mediated current, and a long-lasting DNQX-insensitive current component at +40 mV, typical of NMDAR response. (*Right*) In cortical NR1-null neurons, the NMDA component of this outward current is completely absent (*Upper*), and the remaining fast component of the response is completely blocked by 20 μM DNQX (*Lower*), demonstrating the presence of AMPAR at these synapses in the absence of NMDARs. (*B*) The amplitude of the NMDAR-mediated component was measured at 100 ms poststimulus at a holding potential of +40 mV and was 36.80 ± 6.08 pA ($n = 5$ cells) in WT neurons (black bar) and 1.05 ± 1.86 pA ($n = 6$ cells) in the KO (gray bar), confirming that the genetic deletion is effective in abolishing NMDAR currents. The cumulative data include data from P8 and P9 ($P < 0.01$). (*C*) Traces from whole-cell patch–clamp recordings at −70 mV from WT and cortical NR1-null layer 2/3 pyramidal neurons. Recordings were made in AP5, gabazine, and TTX to selectively record AMPAR-mediated mEPSCs. (*D*) Cortical NR1-null neurons have increased AMPAR mEPSC amplitude (9.5 ± 0.43 pA in the WT and 12.3 ± 0.57 pA in the KOs) ($P <$ 0.01) and frequency (4.4 ± 0.87 Hz in the control and 6.8 ± 0.76 Hz in the KO) ($P < 0.05$). One-minute recordings were analyzed for each cell (11 cells from five animals for each group). Error bars show standard error of the mean. (*E*) Cumulative frequency plots for mEPSC amplitude and interevent interval (time between two consecutive mEPSCs) are shown for 11 analyzed cells from each group. KO neurons have a larger percentage of higher amplitude currents and shorter interevent intervals.

layer 2/3 pyramidal neurons of the somatosensory cortex, which receive direct input from layer 4. Whole-cell patch-clamp recordings were carried out at −70 mV to reveal the AMPA current and at +40 mV to reveal the NMDA + AMPA current. In control neurons, both AMPAR- and NMDAR-mediated EPSCs are clearly present (Fig. 2*A*). In Nex-Cre × floxed NR1 mice, there was a complete absence of the NMDAR component, but a DNQX-sensitive AMPA component was present (Fig. 2*A*), indicating that there are no functional synaptic NMDARs in the cortical conditional NR1-null mice. To further analyze the development of AMPA currents at individual synapses, we recorded spontaneous mEPSCs from layer 2/3 neurons by using whole-cell patch clamp in acute slices from control and cortical NR1-null mice at P19–P21. Recordings were carried out in the presence of TTX, AP5, and gabazine to selectively measure AMPAR-mediated currents. Surprisingly, we found that both the amplitude and frequency of mEPSCs were increased in cortical NR1 KO mice (Fig. 2 *C–E*). These observations indicate that functional AMPAR containing excitatory synapses can develop in the absence of NMDARs, but the AMPAR-mediated current can be influenced by the NMDAR signaling (24, 25).

We next investigated whether the development of dendrites or dendritic spines was affected in cortical NR1-null mice because both of these parameters can affect synaptic function. For these experiments, we perfusion-fixed the brains at different ages between P10 and P20, injected Lucifer yellow into single layer 2/3

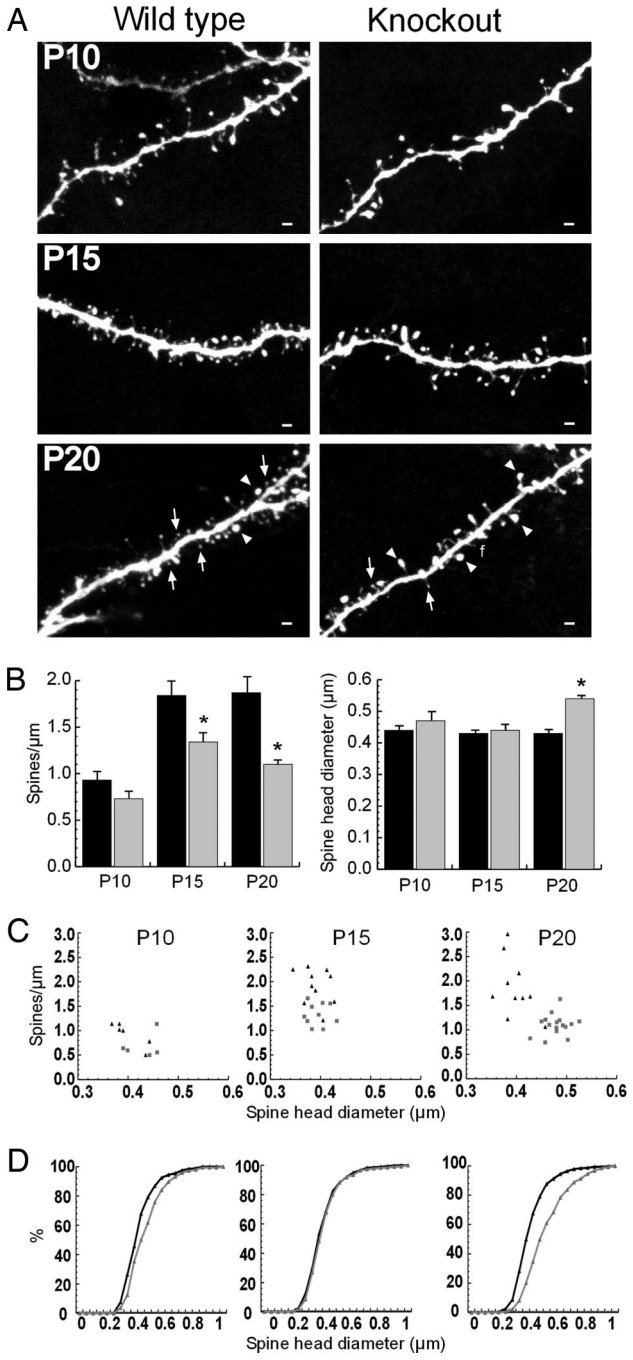

Fig. 3. Effect of loss of NMDAR function on spine morphology and density. (*A*) Representative examples of Lucifer yellow-filled layer 2/3 pyramidal neuron basal dendrites are shown at the three age groups studied. At P15 and P20, lower spine density is evident in NR1-null dendrites when compared with WT. At P20, small-headed spines (arrows), which populate the WT neuron dendrites, are largely absent from the NR1-null neuron dendrites. On NR1-null neuron dendrites, larger-headed spines (arrow heads) are frequently observed, which are rarely seen in the WT. The letter ''f'' on the P20 NR1-null dendrite indicates a dendritic protrusion without a head, similar to a filopodia. These protrusions were infrequent and were not included in the analysis. (Scale bars: 1 μm.) (*B*) Average spine density and spine head diameter analysis in WT and NR1-null cortical layer 2/3 neurons. Spine density is not different at P10 (0.93 $\pm$ 0.1 spine per μm in WT and 0.73 $\pm$ 0.06 spine per μm in NR1 nulls). Spine density is reduced in the NR1-null neurons at P15 (1.8 $\pm$ 0.17 spine per μm in WT and 1.3 $\pm$ 0.05 spine per μm in NR1 nulls) ($P < 0.01$) and at P20 (1.9 $\pm$ 0.35 spine per μm in WT and 1.1 $\pm$ 0.04 spine per μm in NR1 nulls) ($P < 0.01$). Spine density at the P20 KO also was lower when compared with the P15 KO ($P < 0.05$). At P20, spine head diameter was significantly increased in the KO by 25% (WT = 0.43 $\pm$ 0.02 μm and KO = 0.54 $\pm$ 0.01 μm) ($P < 0.01$). Spine head diameter was not significantly different at other age groups. The number of animals and cells, respectively, are as follows: P10 WT, 2, 6; P10 KO, 2, 6; P15 WT, 3, 10; P15 KO, 3, 10; P20 WT, 5, 10; P20 KO, 3, 16. More than 20 spines were analyzed for each cell. Error bars show standard error of the mean. Black bars show WT, and gray bars show NR1 nulls. (*C*) Spine density is plotted against spine head diameter for individual neurons. Each triangle represents a single neuron. WT (black triangles) and NR1-null (gray squares) neurons are plotted for each age group. At P15 and P20, WT neurons have higher spine densities than NR1 nulls. WT and NR1-null neurons have similar spine head diameters at P10 and P15, but the spine head diameter of NR1-null neurons is increased at P20. (*D*) Normalized cumulative frequency plots of spine head diameters analyzed at each age (n = 197, 458, and 642 spines from WT; n = 183, 261, and 633 spines from NR1-null mice at P10, P15, and P20, respectively). The distribution of P20 NR1 KO is skewed toward the right compared with the WT.

pyramidal neurons in the somatosensory cortex, and imaged their basal dendrites by confocal microscopy. Intracellular labeling of layer 2/3 pyramidal neurons, followed by Sholl analysis and total dendritic length measurements of basal dendrites, revealed no major differences between control and cortical NR1-null mice (SI Fig. 7). There also were no apparent effects on the development of the apical dendrite (SI Fig. 7 and data not shown). Although we cannot rule out a potential effect on dendritic branch dynamics, these data suggest that NMDAR function is not required for gross dendritic development of layer 2/3 neurons.

The intracellular labeling method also was effective in delineating spines, and well developed spines were present at all of the ages examined. In control mice, there was an ≈2-fold increase in spine density between P10 and P15, after which spine density was relatively unchanged. The spine density in cortical NR1 nulls was comparable to controls at P10, indicating that the density of spines at this age was not dependent on the presence of functional NMDARs. However, spine density in cortical NR1-null mice at P15 was significantly less than in controls, suggesting that the developmental increase in spine density is positively regulated by functional NMDARs (Fig. 3 *B* and *C*). The difference in spine density between controls and cortical NR1 nulls was even more pronounced by P20, indicating that the difference at P15 was not simply because of delayed spine formation (Fig. 3 *B* and *C*).

Assessment of spine head diameter indicated that, in control neurons, spine size did not significantly change between P10 and P20. The spine size in cortical NR1-null mice was comparable to controls at P10 and P15, but, surprisingly, spine sizes in the KOs was significantly larger than controls at P20 (Fig. 3*B*). Comparing changes in spine density and spine size between control and cortical NR1-null neurons at different developmental times for individual neurons indicates that spine parameters between these two populations are indistinguishable at P10. The normal increase in spine density between P10 and P15 is reduced in NR1-null neurons, but head diameter is not affected at this age. By P20, the spine sizes in NR1-null neurons are considerably larger than controls, with density difference more pronounced (Fig. 3*C*). To determine whether density of spines with smaller head diameters was differentially affected, we made cumulative frequency plots, including all spines analyzed per age group (Fig. 3*D*). We observed that at P10 and P15 spine head diameter distributions were not markedly affected, but at P20 the distribution was shifted toward higher values in NR1-null mice (Fig. 3*D*). These data indicate that spine size is affected across the range of spine head diameters in NR1-null neurons, suggesting that loss of NR1 leads to a general increase in spine head size and cannot be explained simply by a selective loss of the small spines.

To further characterize the differences in spine morphology at P20, we examined the ultrastructure of these spines by high-voltage electron microscopic tomography (EMT) and serial thin

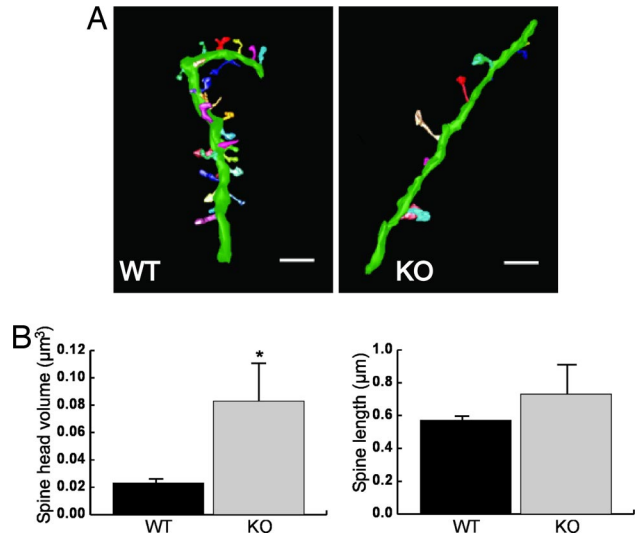

Fig. 4. EM tomography on WT and NR1-null layer 2/3 cortical neurons. (*A*) High-resolution EM tomograms of layer 2/3 dendritic branches from WT and KO mice at P19. Each dendritic protrusion is marked with a different color. The lower density of spines and larger spine heads is observed in the NR1-null sample. (Scale bars: 1 μm.) (*B*) Spine density is 2.98 spine per μm for the WT and 0.99 spine per μm for the NR1-null sample. Spine head volumes are 0.023 $\pm$ 0.004 μm^3 and 0.083 $\pm$ 0.027 μm^3 for the WT (n = 10) and the NR1-null (n = 4) neurons, respectively ($P < 0.01$). Spine lengths were not significantly different (0.57 $\pm$ 0.03 μm and 0.73 $\pm$ 0.18 μm for WT and KO, respectively). *, $P < 0.01$.

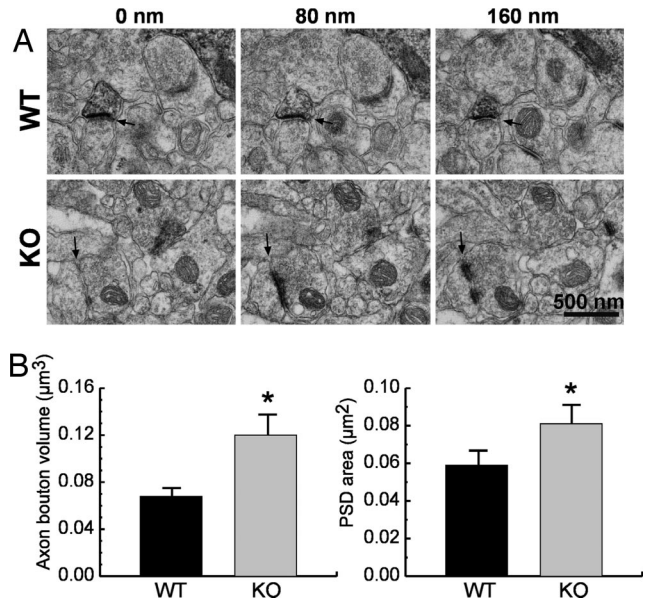

Fig. 5. Cortical NR1-null neurons have increased presynaptic bouton volume and postsynaptic density area. (*A*) Representative serial EM images from WT and cortical NR1-null layer 2/3 cortices. Arrows indicate asymmetric spine synapses in WT and KO samples in consecutive sections. Synapses were outlined through their entire thickness for 3D reconstruction and quantification (data not shown). (*B*) Axon bouton volume was 0.068 $\pm$ 0.01 μm^3 in the WT and 0.12 $\pm$ 0.0014 μm^3 in the KO ($P < 0.01$). The PSD area was 0.059 $\pm$ 0.006 μm^2 in the WT and 0.081 $\pm$ 0.01 μm^2 in the KO ($P < 0.05$). One animal was used for each group; 42 WT and 34 KO synapses were reconstructed and analyzed. Error bars show standard error of the mean. *, $P < 0.05$.

section EM. For EMT, neurons were delineated by filling with Lucifer yellow, photoconverted by diaminobenzadine, and made electron-dense by poststaining with OsO_4. Dendritic spines were segmented from digital slices <10-nm thick within tomographic volumes made from projection datasets of 1-μm-thick sections. Resulting 3D reconstruction recapitulated our light microscopy data, revealing lower density of spines with larger heads in NR1-null neurons (Fig. 4). Dendritic spine head volumes of spines that were fully included in the section depth were measured. Spine head volumes were 0.023 $\pm$ 0.004 μm^3 in WT and 0.083 $\pm$ 0.027 μm^3 in the cortical NR1-null neurons, which is in agreement with the robust increase in head size in NR1 nulls observed at light microscopy. Assuming spherical spine heads, these results would predict 0.36- and 0.54-μm average spine head diameters, compared with our light microscopy measurements of 0.43 and 0.54 μm in WT and KO, respectively. We think the higher average spine head in the WT light microscopy data could be because of our inability to resolve and measure smaller spine heads at light microscopy level.

We next carried out serial thin section electron microscopic reconstructions of filled layer 2/3 neurons from animals at P19–P20 to determine whether we could detect differences in the synaptic ultrastructure between control and NR1-null neurons. Specifically, we measured presynaptic axon terminal bouton volume and PSD area of asymmetric spine synapses in this region because these measures are closely correlated with synaptic function (26). We found that the PSD area in cortical NR1-null neurons was increased by 37%, compared with controls (Fig. 5). We also found that axon bouton volume was increased by 75% in cortical NR1-null neurons, compared with controls (Fig. 5*B*). It has been shown that axon bouton volume is linearly correlated with the number of docked vesicles (26), which comprise the readily releasable pool (RRP) of neurotransmitter (27). An increase in axon bouton volume would predict an increase in RRP and a similar increase in the release probability of each synapse. Such an increase in release probability could account for the observed increase in mEPSC frequency in NR1-null neurons.

One limitation to the interpretation of the observations presented here is that it is difficult to formally prove that the effects observed represent a cell-autonomous role of NMDARs in the postsynaptic neuron because the receptor has been deleted from all excitatory neurons in the cortex, which can affect the network's overall activity. This issue generally affects the interpretation of any pharmacological or genetic manipulation that affects a group of neurons. To investigate the cell autonomy of the effect, we examined the effect of genetic loss of NR1 in individual neurons on the development of spines *in vitro*. As shown in SI Fig. 8, cortical cultures from floxed NR1 mice have well developed spines by 21 days *in vitro* (DIV) as revealed by GFP expression (SI Fig. 8). Excision of NR1 in culture by transfection of Cre recombinase, along with GFP, led to a marked reduction in spine density (SI Fig. 8). This reduction in spine density could be rescued by coexpression of WT NR1, supporting a cell-autonomous role for NR1 in regulating spine density. In addition, an NR1 construct carrying a mutation in the calcium permeability domain was unable to rescue this defect, indicating that calcium influx by NMDA receptors was required for the effects of NMDAR function on spine density. In contrast to our *in vivo* observations, expression of Cre recombinase in floxed NR1 neurons in culture did not lead to an increase in spine head size, and we did not find a consistent increase in AMPAR mini-amplitude or frequency either (data not shown). This finding may reflect either differences in spine regulation *in vivo* and *in vitro* or a cell-nonautonomous role for NR1 in regulating spine volume.

In complementary experiments, we examined the effects of loss of NR1 in hippocampal slice cultures. Hippocampal slices from floxed NR1 mice were cultured at P5 and transfected at 5 DIV with GFP or GFP, together with a plasmid expressing Cre.

The slice cultures were fixed at 11 DIV, and spines on transfected CA1 pyramidal neurons were analyzed by confocal microscopy. As shown in SI Fig. 9, in hippocampal slice cultures, deletion of NR1 by Cre recombinase led to a reduction in spine density without significant alteration of spine head diameter. The experiments in the dissociated cortical cultures and hippocampal slice cultures strongly suggest that NR1 exerts a cell-autonomous role in regulating spine density.

Discussion

The observations reported here reveal a critical role for NMDA receptor signaling in regulating spine development and synaptic function. We find that loss of NR1 leads to a 40% decrease in spine density and to an increase in spine size and the size of presynaptic boutons. These changes are accompanied by an increase in mEPSC amplitudes. The observed reduction in spine density is consistent with previous observations that dendritic protrusions can be triggered by glutamate or LTP-inducing stimuli in an NMDAR-dependent manner in slice cultures (18, 19). It has been reported that new spine formation precedes synapse formation (28) and that newly formed spines preferentially synapse onto preexisting boutons, forming multisynaptic boutons (28–30). If this is generally true, then postsynaptic NMDAR signaling may not be required for spine formation, but instead may be required for spine stability. Recently, it was reported that siRNA-mediated NR1 knockdown in cultures results in unstable spines and reduced spine density (31), supporting a function of NMDA receptor on spine stability. A definitive resolution of this issue will require *in vivo* time-lapse imaging of spine dynamics in WT and cortical NR1 KO mice.

Although the role of NMDAR signaling in spine morphogenesis has been previously explored, genetic manipulations offer certain advantages over *in vitro* and pharmacological experiments. For instance, the *in vivo* significance of experiments carried out in culture can be difficult to determine, and some of the *in vivo* effects may not be seen in culture. Even in our own experiments, the robust effect of loss of NR1 on spine size was not seen in cortical cultures. Similarly, one of the limitations of pharmacological block of NMDARs, which has been used to test the role of NMDARs in cortical development, is that it may not fully capture the function of the receptor because the physical presence of NMDARs also may influence synaptic development. Thus, a genetic approach provides information that cannot easily be inferred from other kinds of experiments.

Our findings on spine density differ with a previous analysis of a conditional NR1-null mouse that was generated by crossing NR1-floxed mice with Emx-Cre mice (32). On the basis of Golgi staining, the authors reported a 20% increase in dendritic spine density in layer 4 cortical neurons (33). Although the basis of the discrepancy between these studies is unclear, one possibility is that loss of NR1 might have different effects on different cell types: layer 4 spiny stellate neurons versus layer 2/3 pyramidal neurons. Also, the difference may be related to differences in experimental techniques. In our study, we used intracellular fills and EM tomography, whereas the previous study used Golgi staining. Another likely explanation is that the efficiency of Cre-mediated DNA recombination may be different in Nex-Cre and Emx-Cre mice. NMDAR loss in the cortical neurons of Emx-Cre mice was not analyzed for each layer specifically. In cortical NR1 KO animals with Emx-Cre, rudimentary patches of barrels are formed, which is because of a lack of selective arborization of thalamocortical axons in layer 4 (32, 34). However, in Nex-Cre-induced NR1 nulls, barrels are completely absent (Fig. 1). The amount of NMDAR function has severe implications on the formation of somatosensory map formation in barrelloids, barrellettes, and barrels in the somatosensory cortex (35). In their study, Iwasato *et al.* (35) rescued NR1 KO animals by expressing different levels of NR1 transgene and observed that axonal segregation into barrels was restored only in higher levels of NR1 expression. Thus, complete lack of barrels in Nex-Cre-induced NR1-null animals could be caused by more efficient and/or earlier deletion of NMDARs than in Emx-Cre-induced NR1 nulls. Therefore, a more efficient NR1 deletion could account for differences in spine density as well.

The second major finding of the study is that NMDAR signaling negatively regulates AMPA currents and spine size. Previous work suggests that pharmacological NMDAR blockage *in vivo* does not alter AMPAR currents in superior colliculus (36), and a similar manipulation *in vitro* results in an initial reduction in AMPAR current, which later recovers (37). Our work is fundamentally different from these studies because it examines the consequences of removal of NMDAR as opposed to loss of NMDAR activity. Previously, AMPAR currents were shown to be present in NR1 KO animals (38, 39), but they were not analyzed in detail. We find that loss of NR1 leads to an increase in AMPA mEPSC amplitude. This effect of NMDARs on AMPA currents might explain the low AMPAR:NMDAR ratio seen in developing synapses. One important difference between developing and mature synapses is the relative contribution of NR2A and NR2B receptors to NMDAR-mediated currents. Developing synapses mainly contain NR1 and NR2B subunits (40, 41). As synapses mature, NR2A receptors are incorporated into the synapses such that much of the NMDAR current in adults is carried by NR2A-containing receptors (40). An interesting possibility is that signaling by NR1-NR2B receptors might inhibit incorporation of AMPARs or remove AMPARs from newly formed synapses, whereas signaling by NR1-NR2A receptors might favor AMPAR incorporation as the synapse matures. In fact, such a restrictive role of NR2B receptors has recently been reported and may explain the observed increase in AMPAR currents in NR1-null neurons (25). It should be noted, however, that NR2B also is implicated in LTP-mediated AMPAR incorporation into synapses (24). Thus, the effect of NMDAR signaling on AMPAR currents could be dependent on the level of afferent activity.

We also find that there is an increase in spine size in cortical NR1-null neurons. Although the mechanism underlying this effect remains to be identified, one possibility is that the increase in AMPAR currents in NR1-null neurons may cause the observed increase in spine size in NR1-null neurons. This finding would be consistent with reports that overexpression of GluR2 is sufficient to induce an increase in spine size in hippocampal neurons (42). Another possibility is that the increase in both AMPAR currents and spine size represents a homeostatic response to the reduction in spine density in NR1-null neurons. This finding would be consistent with the observation that the reduction in spine density is observed by P15, but the increase in spine size is not seen until P20. Independent of the precise mechanism by which NMDAR signaling exerts its effect, our observations provide definitive evidence that NMDAR function plays an important role in regulating spine size and density *in vivo*.

Materials and Methods

Transgenic Mice. Cortical NR1 KO mice were obtained by crossing NR1-floxed mice, in which LoxP sites were inserted in between exons 10 and 11 and downstream of 3′ end (20, 32), and Nex-Cre mice (21), which express Cre recombinase in cortical pyramidal neurons. NR1flox/+;NexCre/+ mice were crossed with each other to obtain NR1flox/NR1flox;NexCre/+ or NR1flox/NR1flox;NexCre/NexCre mice, which we refer to as the cortical NMDAR KO mice or KO mice. Mice that are heterozygous for NR1flox allele or lack Cre gene are used as controls and referred to as WT.

Electrophysiology. Mice ages P10–P21 were anesthetized before being killed. Then 300-μm-thick brain slices of the somatosensory cortex were obtained by vibratome sectioning. AMPAR-mediated mEPSCs recordings were done at -70 mV in ACSF containing 1 μM tetrodotoxin, 100 μM AP5, and 10 μM gabazine. For layers 4 to 2/3 stimulations, concentric bipolar stimulation electrodes were placed on layer 4 directly below the recorded cell.

Lucifer Yellow Injection. Brains were perfused with Ringer's solution, followed by 4% paraformaldehyde (PFA) and 0.1% glutaraldehyde in 0.1M PBS warmed to 37°C and postfixed in 4% PFA for 1 h on ice. Then 100-μm-thick slices were obtained, and neurons were filled with Lucifer yellow (5%) by using sharp electrodes under visual guidance. Confocal microscopy was used to image dendritic spines, and analyses were done by using a custom plugin in ImageJ.

EM: Serial Thin Sections. Lucifer yellow in filled cells was excited at 488-nm illumination by using a Xenon lamp to photooxidize diaminobenzidine into a brownish reaction product. After further processing, including postfixation with OsO_4, sections were dehydrated and embedded in Durcupan ACM resin (Electron Microscopy Sciences). Then 80-nm serial sections were obtained, imaged by using a JEOL 1200EX, aligned, and used for measuring PSD area and axon bouton volume. For EMT, 1- to 5-μm-thick sections were cut with an ultramicrotome and mounted on clam shell EM grids. Sections were decorated with 10 + 20-nm colloidal gold particles (to serve later as fiducial marks for tomographic alignment) and carbon-coated on both sides. The 4- to 5-μm-thick sections were sent to Osaka, Japan, for tomographic imaging by using the 3 MeV Hitachi H3000U ultra-high voltage EM. Dendritic shafts and spines in the digital slices from the tomograms were segmented, 3D-reconstructed, and measured by using IMOD and NCMIR's in-house reconstruction algorithm called TxBR (43). Spine head volumes and spine lengths were analyzed for protrusions that are entirely included in the tomograms.

For detailed methods including Western blots, immunohistochemistry, and cytochrome oxidase staining, see *SI Materials and Methods*.

We thank Drs. S. Tonegawa (Massachusetts Institute of Technology, Cambridge, MA) and K. Nave (Max Planck Institute, Goettingen, Germany) for kindly providing us with the transgenic mice; Tom Maddock for writing an ImageJ plugin that was used for spine measurements; Masako Terada and James Obayashi for EMT processing; and the A.G. Laboratory members for discussion and comments. This work was supported by a National Institute of Mental Health grant (to A.G.), the University of California at San Diego Kavli Institute for Mind and Brain (A.G.), the National Alliance for Research on Schizophrenia and Depression (S.K.U.), National Institutes of Health Grant P41-RR04050 (to M.E.), and the National Center for Microscopy and Imaging Research.

1. Harris KM, Kater SB (1994) *Ann Rev Neurosci* 17:341–371.
2. Yuste R, Bonhoeffer T (2001) *Ann Rev Neurosci* 24:1071–1089.
3. Nimchinsky EA, Sabatini BL, Svoboda K (2002) *Ann Rev Physiol* 64:313–353.
4. Portera-Cailliau C, Pan DT, Yuste R (2003) *J Neurosci* 23:7129–7142.
5. Fiala JC, Feinberg M, Popov V, Harris KM (1998) *J Neurosci* 18:8900–8911.
6. Fischer M, Kaech S, Knutti D, Matus A (1998) *Neuron* 20:847–854.
7. Konur S, Yuste R (2004) *J Neurobiol* 59:236–246.
8. Park M, Penick EC, Edwards JG, Kauer JA, Ehlers MD (2004) *Science* 305:1972–1975.
9. Matsuzaki M, Honkura N, Ellis-Davies GC, Kasai H (2004) *Nature* 429:761–766.
10. Zhou Q, Homma KJ, Poo MM (2004) *Neuron* 44:749–757.
11. Petralia RS, Esteban JA, Wang YX, Partridge JG, Zhao HM, Wenthold RJ, Malinow R (1999) *Nature Neurosci* 2:31–36.
12. Malinow R, Malenka RC (2002) *Ann Rev Neurosci* 25:103–126.
13. Zhu JJ, Esteban JA, Hayashi Y, Malinow R (2000) *Nature Neurosci* 3:1098–1106.
14. Isaac JT, Crair MC, Nicoll RA, Malenka RC (1997) *Neuron* 18:269–280.
15. Wu G, Malinow R, Cline HT (1996) *Science* 274:972–976.
16. Isaac JT (2003) *Neuropharmacology* 45:450–460.
17. Saglietti L, Dequidt C, Kamieniarz K, Rousset MC, Valnegri P, Thoumine O, Beretta F, Fagni L, Choquet D, Sala C, *et al.* (2007) *Neuron* 54:461–477.
18. Engert F, Bonhoeffer T (1999) *Nature* 399:66–70.
19. Maletic-Savatic M, Malinow R, Svoboda K (1999) *Science* 283:1923–1927.
20. Tsien JZ, Huerta PT, Tonegawa S (1996) *Cell* 87:1327–1338.
21. Wu SX, Goebbels S, Nakamura K, Nakamura K, Kometani K, Minato N, Kaneko T, Nave KA, Tamamaki N (2005) *Proc Natl Acad Sci USA* 102:17172–17177.
22. Kashani AH, Qiu Z, Jurata L, Lee SK, Pfaff S, Goebbels S, Nave KA, Ghosh A (2006) *J Neurosci* 26:8398–8408.
23. Fukaya M, Kato A, Lovett C, Tonegawa S, Watanabe M (2003) *Proc Natl Acad Sci USA* 100:4855–4860.
24. Barria A, Malinow R (2005) *Neuron* 48:289–301.
25. Kim MJ, Dunah AW, Wang YT, Sheng M (2005) *Neuron* 46:745–760.
26. Schikorski T, Stevens CF (1999) *Proc Natl Acad Sci USA* 96:4107–4112.
27. Schikorski T, Stevens CF (2001) *Nature Neurosci* 4:391–395.
28. Knott GW, Holtmaat A, Wilbrecht L, Welker E, Svoboda K (2006) *Nature Neurosci* 9:1117–1124.
29. Toni N, Buchs PA, Nikonenko I, Bron CR, Muller D (1999) *Nature* 402:421–425.
30. Fiala JC, Allwardt B, Harris KM (2002) *Nature Neurosci* 5:297–298.
31. Alvarez VA, Ridenour DA, Sabatini BL (2007) *J Neurosci* 27:7365–7376.
32. Iwasato T, Datwani A, Wolf AM, Nishiyama H, Taguchi Y, Tonegawa S, Knopfel T, Erzurumlu RS, Itohara S (2000) *Nature* 406:726–731.
33. Datwani A, Iwasato T, Itohara S, Erzurumlu RS (2002) *Mol Cell Neurosci* 21:477–492.
34. Lee LJ, Iwasato T, Itohara S, Erzurumlu RS (2005) *J Compar Neurol* 485:280–292.
35. Iwasato T, Erzurumlu RS, Huerta PT, Chen DF, Sasaoka T, Ulupinar E, Tonegawa S (1997) *Neuron* 19:1201–1210.
36. Colonnese MT, Shi J, Constantine-Paton M (2003) *J Neurophysiol* 89:57–68.
37. Zhu JJ, Malinow R (2002) *Nature Neurosci* 5:513–514.
38. Li Y, Erzurumlu RS, Chen C, Jhaveri S, Tonegawa S (1994) *Cell* 76:427–437.
39. Okabe S, Vicario-Abejon C, Segal M, McKay RD (1998) *Euro J Neurosci* 10:2192–2198.
40. Sheng M, Cummings J, Roldan LA, Jan YN, Jan LY (1994) *Nature* 368:144–147.
41. Monyer H, Burnashev N, Laurie DJ, Sakmann B, Seeburg PH (1994) *Neuron* 12:529–540.
42. Passafaro M, Nakagawa T, Sala C, Sheng M (2003) *Nature* 424:677–681.
43. Lawrence A, Bouwer JC, Perkins G, Ellisman MH (2006) *J Struct Biol* 154:144–167.